Paper 2

Proceedings of the Eleventh International Conference
on Computational Structures Technology,
B.H.V. Topping, (Editor),
Civil-Comp Press, Stirlingshire, Scotland

Interactive Buckling of Thin-Walled I-Section Columns

M.A. Wadee and L. Bai
Department of Civil and Environmental Engineering
Imperial College London, United Kingdom

Abstract

An analytical model that describes a thin-walled I-section column under pure compression based on variational principles is presented. The Rayleigh–Ritz method is combined with continuous displacement functions to formulate the total potential energy that is minimized. A system of differential and integral equilibrium equations is formulated for the structural component for which numerical continuation reveals progressive cellular buckling (or *snaking*) arising from the nonlinear interaction between the weakly stable overall mode and the strongly stable local buckling mode. The resulting behaviour is highly unstable and is postulated to be highly sensitive to initial geometric imperfections.

Keywords: buckling, mode interaction, snaking, thin-walled components, nonlinearity.

1 Introduction

The buckling of struts and columns represents the most common type of structural instability problem [1]. However, when the compression member is made from slender metallic plate elements they are well known to suffer from a variety of different elastic instability phenomena. In the current work, the classic problem of a column under axial compression made from a linear elastic material with an open and doubly-symmetric cross-section – an "I-section" – is studied in detail from an analytical approach. Under this type of loading, long members are primarily susceptible to a global (or overall) mode of instability namely Euler buckling, where flexure about the weak axis occurs once the theoretical Euler buckling load is reached. However, when the individual plate elements of the column cross-section, namely the flanges and the web, are relatively thin or slender, elastic local buckling of these may also occur; if this happens in combination with the overall instability, then the resulting behaviour is usually far more unstable than when the modes are triggered individually. Recent work on the interactive buckling of columns include experimental and finite element studies [2, 3], where the focus was on the behaviour of columns made from stainless steel. However, the more generic finding that the members had an increased sensitivity to imperfections was highlighted. Other structural components that are known to suffer from the interaction of local and overall instability modes are thin-walled beams under uniform bending [4], sandwich struts [5], stringer-stiffened and corrugated plates [6, 7] and built-up, compound or reticulated columns [8].

Apart from the aforementioned work where some successful numerical modelling was presented [3], the formulation of a mathematical model accounting for the interactive behaviour has not been forthcoming. The current work presents the development of a variational model that accounts for the mode interaction between overall Euler buckling and local buckling of a flange such that the perfect elastic post-buckling response of the column can be evaluated. A system of nonlinear ordinary differential equations subject to integral constraints is derived, which are solved using the numerical continuation package AUTO [9]. It is indeed found that the system is highly unstable when interactive buckling is triggered; snap-backs in the response showing sequential destabilization and restabilization and a progressive spreading of the initial localized buckling mode are also revealed. This latter type of response has become known in the literature as *cellular buckling* [10] or *snaking* [11] and it is shown to appear naturally in the numerical results of the current model. As far as the authors are aware, this is the first time this phenomenon has been found in columns undergoing Euler and local buckling simultaneously. Similar behaviour has been discovered in various other mechanical systems such as in the post-buckling of cylindrical shells [12], the sequential folding of geological layers [13] and most recently in the lateral buckling of thin-walled beams [4].

Experimental results from the literature [2] are used primarily as a guideline for the current study. Highly encouraging results emerge both in terms of the mechanical destabilization exhibited and the nature of the post-buckling deformation. This demonstrates that the fundamental physics of this system is captured by the analytical approach. Currently, the situation where overall buckling occurs first is catered for; hence, a brief discussion is presented on how the current model could be enhanced to allow for the case where local buckling is critical. Conclusions are then drawn.

2 Analytical Model

Consider a thin-walled I-section column (or strut) of length L made from a linear elastic, homogeneous and isotropic material with Young's modulus E and Poisson's ratio ν. It is assumed to have a perfect geometry and is loaded by an axial force P (see Figure 1) that is applied at the centroid of the cross-section (Figure 2) with rigid end plates that transfer the force uniformly to the entire cross-section. The web is assumed to provide a simple support to both flanges and not to buckle under the axial

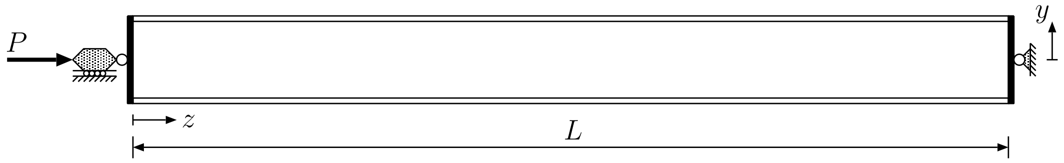

Figure 1: Elevation of an I-section strut of length L that is compressed axially by a force P. The longitudinal and lateral coordinates are z and y respectively.

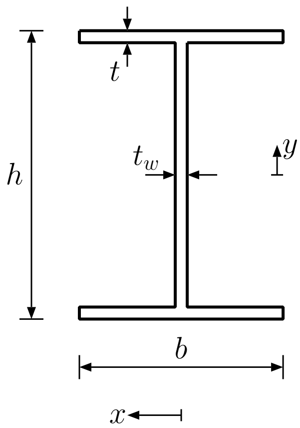

Figure 2: Cross-section of strut; the transverse coordinate is x.

compression, an assumption that is justified later. For the current case, each flange has width b and thickness t, the total cross-section depth is h and the column length L is chosen such that Euler buckling about the weaker y-axis occurs place before any flange buckles locally. It is assumed currently that the I-section is effectively made up from two channel sections connected back-to-back; hence, the assumption is that the web thickness $t_w = 2t$, this type of arrangement has been used in recent experimental studies [2, 4]. The formulation begins with the definitions for both the overall and the local modal displacements. Timoshenko beam theory is assumed, meaning that the effect of shear is not neglected as in standard Euler–Bernoulli beam theory. Although it turns out that the effect of shear is only minor, it is necessary to account for it since it provides the key expressions within the total potential energy equation that allow buckling mode interaction to be modelled [5, 4]. To account for shear, two generalized coordinates q_s and q_t, defined as the amplitudes of the degrees of freedom known as "sway" and "tilt" [5] are introduced to model the overall mode as shown in Figure 3, where the lateral deflection W and the rotation θ are given by the following expressions:

$$\begin{aligned} W(z) &= q_s L \sin \frac{\pi z}{L}, \\ \theta(z) &= q_t \pi \cos \frac{\pi z}{L}. \end{aligned} \tag{1}$$

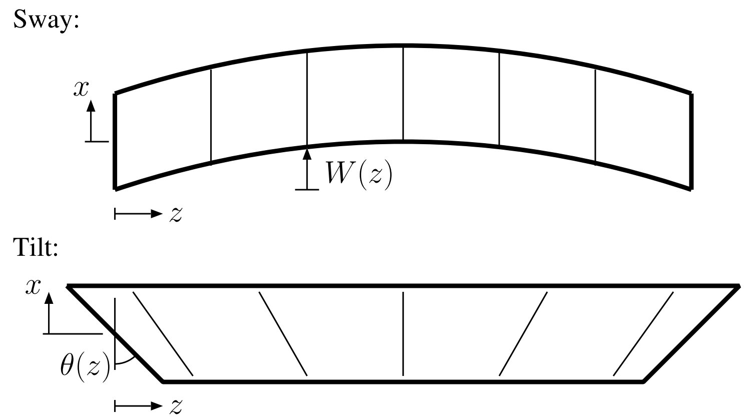

Figure 3: Sway and tilt components of the minor axis overall buckling mode.

For the present case, the shear strain γ_{xz} is included and given by the following expression:

$$\gamma_{xz} = \frac{\mathrm{d}W}{\mathrm{d}z} - \theta = (q_s - q_t)\,\pi \cos\frac{\pi z}{L}. \tag{2}$$

Of course, Euler–Bernoulli beam theory would imply that since $\gamma_{xz} = 0$, then $q_s = q_t$.

The local mode is modelled with appropriate boundary conditions. The outstands of the flanges have free edges, whereas the web is assumed to provide no more than a simple support to the flanges; hence, a linear distribution is assumed in the x direction, see Figure 4), as [14] shows that the local buckling eigenmode would have a linear

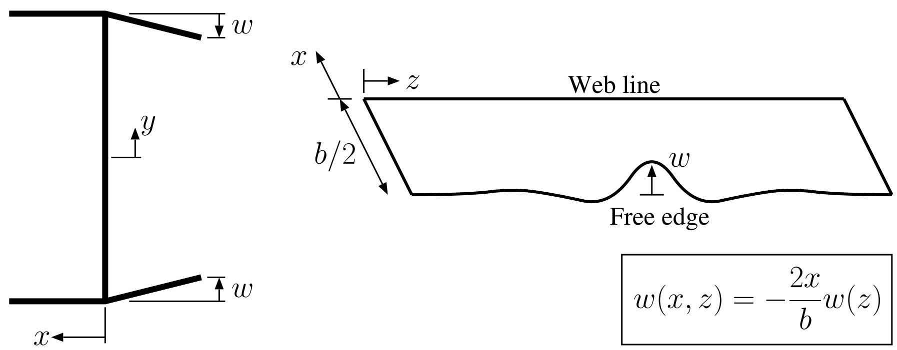

Figure 4: Local buckling mode: out-of-plane flange displacement $w(z)$; note the linear distribution in x direction.

transverse displacement distribution for that type of plate. For the local mode in-plane displacement u, the distribution is also assumed to be linear in x, as shown in Figure 5, leading to the following expressions for the local out-of-plane deflection w and the in-plane deflection u:

$$\begin{aligned} w(z,x) &= -\frac{2x}{b}w(z), \\ u(z,x) &= -\frac{2x}{b}u(z). \end{aligned} \tag{3}$$

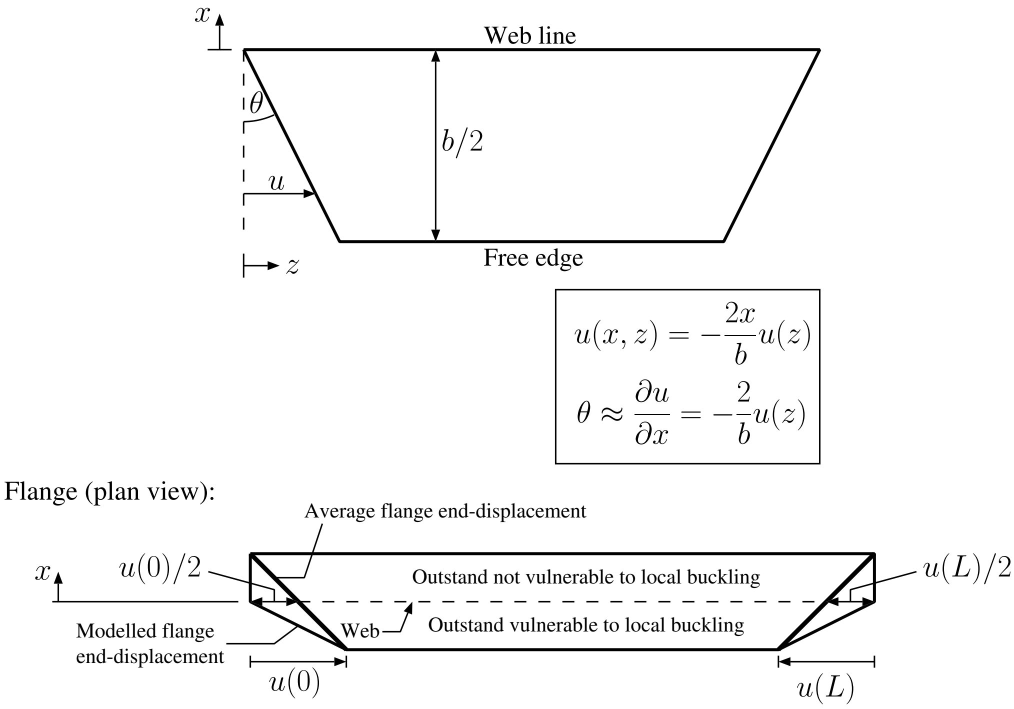

Figure 5: Local buckling mode: in-plane flange displacement $u(z)$; note the linear distribution in x direction and the assumed average end-displacement that is used to calculate the local contribution to the work done by P (lower diagram).

The transverse deflection $v(z, x)$ is assumed to be small and hence neglected for the current case; this reflects the findings from Koiter and Pignataro [6] for rectangular plates with three pinned edges and one free edge.

2.1 Total potential energy

The total potential energy, V, was determined with the main contributions being the overall and local bending energy U_{bo} and U_{bl} respectively, the membrane energy U_m, the shear strain energy U_s and the work done $P\mathcal{E}$. Note that the overall bending energy U_{bo} only consists of the bending energy stored in the web, since the membrane energy stored in the flanges already accounts for the effect of bending in the flanges. The overall bending energy involves the second derivative of W and is given by:

$$
\begin{aligned}
U_{bo} &= \frac{1}{2} E I_w \int_0^L \ddot{W}^2 \, \mathrm{d}z \\
&= \frac{1}{2} E I_w \int_0^L q_s^2 \frac{\pi^4}{L^2} \sin^2 \frac{\pi z}{L} \, \mathrm{d}z,
\end{aligned} \tag{4}
$$

where dots represent differentiation with respect to z and $I_w = 2t(h - 2t)^2/12$ is the second moment of area of the web about the global weak axis. The local bending energy, accounting for both flanges, is determined as:

$$
\begin{aligned}
U_{bl} &= \int_0^L \int_{-b/2}^0 D \left\{ \left[\frac{\partial^2 w}{\partial z^2} + \frac{\partial^2 w}{\partial x^2} \right]^2 - 2(1-\nu) \left[\frac{\partial^2 w}{\partial z^2} \frac{\partial^2 w}{\partial x^2} - \left(\frac{\partial^2 w}{\partial z \partial x} \right)^2 \right] \right\} \mathrm{d}x \, \mathrm{d}z \\
&= D \int_0^L \left[\frac{1}{6} b \ddot{w}^2 + \frac{4}{b} (1-\nu) \dot{w}^2 \right] \mathrm{d}z,
\end{aligned}
\tag{5}
$$

where $D = Et^3/[12(1-\nu^2)]$ is the plate flexural rigidity and ν is the Poisson's ratio. Note that the local bending energy only arises from the more compressive side of the flanges after Euler buckling occurs. The buckled configuration of the flange plate involves double curvature in the z and x directions, indicating the non-developable nature of plate deformation. The so-called membrane strain energy is derived from considering the axial stresses in the flanges, thus:

$$
U_m = \frac{1}{2} E \int_0^L \int_0^t \int_{-b/2}^{b/2} \left(\varepsilon_z^2 + \varepsilon_x^2 + 2\nu \varepsilon_z \varepsilon_x \right) \mathrm{d}x \, \mathrm{d}y \, \mathrm{d}z. \tag{6}
$$

The transverse component of strain ε_x is neglected since it has been shown that it has no effect on the post-buckling behaviour of a long plate with three simply-supported edges and one free edge [6]. The longitudinal strain ε_z has to be modelled separately for different outstand flanges. Recall that the tilt component of the in-plane displacement from the overall mode is given by $u_t = -\theta x$; hence:

$$
\varepsilon_{z,\mathrm{overall}} = \frac{\partial u_t}{\partial z} = x q_t \frac{\pi^2}{L} \sin \frac{\pi z}{L}. \tag{7}
$$

The local mode contribution is based on von Kárman plate theory. A pure in-plane compressive strain Δ is also included. The direct strains in the tension and compression side of the flanges, denoted as ε_{zt} and ε_{zc} are thus:

$$
\begin{aligned}
\varepsilon_{zt} &= x q_t \frac{\pi^2}{L} \sin \frac{\pi z}{L} - \Delta, \\
\varepsilon_{zc} &= x q_t \frac{\pi^2}{L} \sin \frac{\pi z}{L} - \Delta + \frac{\partial u}{\partial z} + \frac{1}{2} \left(\frac{\partial w}{\partial z} \right)^2 \\
&= x q_t \frac{\pi^2}{L} \sin \frac{\pi z}{L} - \Delta - \frac{2x}{b} \dot{u} + \frac{2x^2}{b^2} \dot{w}^2.
\end{aligned}
\tag{8}
$$

The total membrane energy is thus, assuming that $h \gg t$:

$$
\begin{aligned}
U_m = \int_0^L \Bigg\{ & Eth\Delta^2 + Etb \left[\frac{b^2}{12} {q_t}^2 \frac{\pi^4}{L^2} \sin^2 \frac{\pi z}{L} + \Delta^2 + \frac{1}{6} \dot{u}^2 + \frac{1}{40} \dot{w}^4 \right. \\
& \left. - \frac{b}{2} q_t \frac{\pi^2}{L} \sin \frac{\pi z}{L} \left(\frac{1}{3} \dot{u} + \frac{1}{8} \dot{w}^2 \right) - \frac{1}{2} \dot{u} \Delta - \frac{1}{6} \dot{w}^2 \Delta + \frac{1}{8} \dot{u} \dot{w}^2 \right] \Bigg\} \mathrm{d}z,
\end{aligned}
\tag{9}
$$

where, apart from the first term that represents the energy stored in the web, the contributions are from the strains in both flanges. The shear strain energy U_s has a general expression:

$$U_s = \frac{1}{2} G \int_0^L \int_0^t \int_{-b/2}^{b/2} \gamma_{xz}^2 \, \mathrm{d}x \, \mathrm{d}y \, \mathrm{d}z, \tag{10}$$

where G is the shear modulus and is given by $E/[2(1+\nu)]$ for a homogeneous and isotropic material. The shear strain γ_{xz} contributions are also modelled separately for the compression and the tension side of the flanges:

$$\begin{aligned} \gamma_{xzt} &= \frac{\partial W}{\partial z} - \theta = (q_s - q_t)\, \pi \cos \frac{\pi z}{L}, \\ \gamma_{xzc} &= \frac{\partial W}{\partial z} - \theta + \frac{\partial u}{\partial x} + \frac{\partial w}{\partial z} \frac{\partial w}{\partial x} \\ &= (q_s - q_t)\, \pi \cos \frac{\pi z}{L} - \frac{2}{b} u + \frac{4}{b^2} x w \dot{w}. \end{aligned} \tag{11}$$

The expression for the strain energy from shear is thus:

$$\begin{aligned} U_s = Gtb \int_0^L \Bigg[& (q_s - q_t)^2 \pi^2 \cos^2 \frac{\pi z}{L} + \frac{2}{b^2} \left(u^2 + \frac{1}{3} w^2 \dot{w}^2 + u w \dot{w} \right) \\ & - \frac{1}{b} (q_s - q_t)\, \pi \cos \frac{\pi z}{L} \left(2u + w \dot{w} \right) \Bigg] \mathrm{d}z. \end{aligned} \tag{12}$$

Finally, the work done by the axial load P is given by:

$$P\mathcal{E} = P \int_0^L \left[\frac{1}{2} q_s \pi^2 \cos^2 \frac{\pi z}{L} - \frac{1}{2} \dot{u} + \Delta \right] \mathrm{d}z, \tag{13}$$

where $\mathcal{E}$ consists of the longitudinal displacement due to overall buckling, the in-plane displacement due to local buckling and the initial end shortening. Note that the displacement due to local buckling is taken as the average value between the maximum in-plane displacement in the more compressed outstand u and the zero in-plane displacement in the less compressed outstand, which is illustrated in Figure 5. The total potential energy V is therefore assembled thus:

$$V = U_{bo} + U_{bl} + U_m + U_s - P\mathcal{E}. \tag{14}$$

2.2 Variational Formulation

The governing differential equations are obtained by performing the calculus of variations on the total potential energy V following a well established procedure that has been detailed in [5]. The integrand of the total potential energy V can be expressed as the Lagrangian ($\mathcal{L}$) of the form:

$$V = \int_0^L \mathcal{L}\left(\ddot{w}, \dot{w}, w, \dot{u}, u, z \right) \mathrm{d}z. \tag{15}$$

The first variation of V is given by:

$$\delta V = \int_0^L \left[\frac{\partial \mathcal{L}}{\partial \ddot{w}} \delta \ddot{w} + \frac{\partial \mathcal{L}}{\partial \dot{w}} \delta \dot{w} + \frac{\partial \mathcal{L}}{\partial w} \delta w + \frac{\partial \mathcal{L}}{\partial \dot{u}} \delta \dot{u} + \frac{\partial \mathcal{L}}{\partial u} \delta u \right] \mathrm{d}z. \tag{16}$$

To find the equilibrium states, V must be stationary, which requires the first variation δV to vanish for any small change in w and u. By assuming that $\delta \ddot{w} = \mathrm{d}(\delta \dot{w})/\,\mathrm{d}z$, $\delta \dot{w} = \mathrm{d}(\delta w)/\mathrm{d}z$ and similarly $\delta \dot{u} = \mathrm{d}(\delta u)/\mathrm{d}z$, integration by parts allows the development of the Euler–Lagrange equations for w and u; these comprise a fourth order differential equation in terms of w and a second order differential equation in terms of u was obtained. For the equations to be solved by the continuation package AUTO, the system has to be non-dimensionalized with respect to the non-dimensional spatial coordinate $\tilde{z}$, which is defined as $\tilde{z} = 2z/L$. The non-dimensional out-of-plane displacement $\tilde{w}$ and in-plane displacement $\tilde{u}$ are also introduced as the scalings $2w/L$ and $2u/L$ respectively. Note that these scalings assume symmetry about the midspan and the differential equations are solved for half the length of the column; this assumption has been shown to be perfectly acceptable for cases where the overall buckling is critical [5, 4]. The non-dimensional differential equations are thus:

$$\begin{aligned}
&\ddddot{\tilde{w}} - \frac{3}{8}\tilde{G}\left[2\phi^2 \tilde{w}\left(\frac{1}{3}\dot{\tilde{w}}^2 + \frac{1}{3}\tilde{w}\ddot{\tilde{w}} + \frac{1}{2}\dot{\tilde{u}}\right) + (q_s - q_t)\frac{\pi^2 \phi}{2}\sin\frac{\pi \tilde{z}}{2}\tilde{w}\right] - 6\phi^2(1-\nu)\ddot{\tilde{w}} \\
&\quad + \frac{3}{8}\tilde{D}\left[q_t \frac{\pi^2}{4\phi}\left(\sin\frac{\pi\tilde{z}}{2}\ddot{\tilde{w}} + \frac{\pi}{2}\cos\frac{\pi\tilde{z}}{2}\dot{\tilde{w}}\right) - \frac{3}{5}\dot{\tilde{w}}^2\ddot{\tilde{w}} + \frac{2}{3}\ddot{\tilde{w}}\Delta - \frac{1}{2}\left(\ddot{\tilde{u}}\dot{\tilde{w}} + \dot{\tilde{u}}\ddot{\tilde{w}}\right)\right] = 0, \\
&\ddot{\tilde{u}} - \frac{3G\phi}{E}\left[\phi\left(\frac{1}{2}\tilde{w}\ddot{\tilde{w}} + \tilde{u}\right) - (q_s - q_t)\pi\cos\frac{\pi\tilde{z}}{2}\right] - \left[q_t\frac{\pi^3}{4\phi}\cos\frac{\pi\tilde{z}}{2} - \frac{3}{4}\dot{\tilde{w}}\ddot{\tilde{w}}\right] = 0,
\end{aligned} \tag{17}$$

where $\tilde{D} = EtL^2/D$, $\tilde{G} = GtL^2/D$ and $\phi = L/b$. Equilibrium also requires the minimization of V with respect to the generalized coordinates q_s, q_t and Δ. This essentially provides three integral conditions, again expressed in non-dimensional form:

$$\begin{aligned}
\frac{\partial V}{\partial q_s} &= \pi^2 q_s + \tilde{s}(q_s - q_t) - \frac{PL^2 q_s}{EI_w} - \frac{\tilde{s}\phi}{\pi}\int_0^1 \cos\frac{\pi\tilde{z}}{2}\left(\frac{1}{2}\tilde{w}\dot{\tilde{w}} + \tilde{u}\right)\mathrm{d}\tilde{z} = 0, \\
\frac{\partial V}{\partial q_t} &= \pi^2 q_t - \tilde{k}(q_s - q_t) + \phi\int_0^1 \left[\frac{\tilde{k}}{\pi}\cos\frac{\pi\tilde{z}}{2}\left(\frac{1}{2}\tilde{w}\dot{\tilde{w}} + \tilde{u}\right)\right. \\
&\qquad \left. - \sin\frac{\pi\tilde{z}}{2}\left(2\dot{\tilde{u}} + \frac{3}{4}\dot{\tilde{w}}^2\right)\right]\mathrm{d}\tilde{z} = 0, \\
\frac{\partial V}{\partial \Delta} &= \int_0^1 \left[2\left(1 + \frac{h}{b}\right)\Delta - \frac{1}{2}\dot{u} - \frac{1}{6}\ddot{w}^2 - \frac{P}{Etb}\right]\mathrm{d}\tilde{z} = 0,
\end{aligned} \tag{18}$$

where $\tilde{s} = (2GtbL^2)/(EI_w)$ and $\tilde{k} = (12GL^2)/(Eb^2)$. The boundary conditions for $\tilde{w}$ and $\tilde{u}$ and their derivatives are for pinned end conditions for $\tilde{x} = 0$ and for symmetry at $\tilde{x} = 1$:

$$\tilde{w}(0) = \ddot{\tilde{w}}(0) = \dot{\tilde{w}}(1) = \dddot{\tilde{w}}(1) = \tilde{u}(1) = 0, \tag{19}$$

with a further condition from matching the in-plane strain:

$$\frac{1}{3}\tilde{u}(0) + \frac{1}{8}\tilde{w}^2(0) - \frac{1}{2}\Delta + \frac{P}{2Etb} = 0 \tag{20}$$

Linear eigenvalue analysis is conducted to determine the critical load for overall buckling P_o^{C}. This is achieved by considering the Hessian matrix V_{ij}, thus:

$$V_{ij} = \begin{bmatrix} \frac{\partial^2 V}{\partial {q_s}^2} & \frac{\partial^2 V}{\partial q_s \partial q_t} \\ \frac{\partial^2 V}{\partial q_t \partial q_s} & \frac{\partial^2 V}{\partial {q_t}^2} \end{bmatrix}; \tag{21}$$

at the critical load V_{ij} is singular. Hence, the critical load for overall buckling is:

$$P_o^{\mathrm{C}} = \frac{\pi^2 E I_w}{L^2} + \frac{2Gtb}{1+\tilde{k}}. \tag{22}$$

3 Numerical example and discussion

The full nonlinear non-autonomous differential equations are obviously complicated to be solved analytically. The continuation and bifurcation software AUTO-07P has been shown in the literature [4, 5] to be an ideal tool to solve the equations numerically. For this type of mechanical problem, one of its major attributes is that it has the capability to show the evolution of the solutions to the equations with parametric changes. The solver is very powerful in locating bifurcations and tracing branching paths as model parameters are varied. To demonstrate this, an example set of section properties are chosen which are shown in Table 1. The overall critical load P_o^{C} can

Column length L	4000 mm
Flange width b	96 mm
Flange thickness t	1.2 mm
Section depth h	120 mm
Section area A	$513\ \mathrm{mm}^2$
Young's modulus E	$210\ \mathrm{kN/mm}^2$
Poisson's ratio ν	0.3

Table 1: Section and material properties. Recall that the thickness of the web $t_w = 2t$. The section properties are identical to those tested in [2].

be calculated using Equation (22), whereas the local buckling critical stress σ^{C} can be evaluated using the well-known formula $\sigma^{\mathrm{C}} = kD\pi^2/b^2t$, where the coefficient k depends on plate boundary conditions; approximate values being $k = 0.43$ and $k = 4$ are chosen for the flanges and the web respectively, assuming that the plates are relatively long [14]. Table 2 summarized the critical loads and showed the assigned section dimensions satisfy the assumptions that the overall mode is critical and that the critical load of the web is orders of magnitude higher than that of the flange.

Average overall buckling stress	σ_o^{C}	$44.7\ \mathrm{N/mm^2}$
Flange local buckling stress	$\sigma_{l,\mathrm{flange}}^{\mathrm{C}}$	$51.1\ \mathrm{N/mm^2}$
Web local buckling stress	$\sigma_{l,\mathrm{web}}^{\mathrm{C}}$	$2731\ \mathrm{N/mm^2}$

Table 2: Theoretical values of the overall and local critical buckling stresses. Note that the overall buckling mode would be triggered first, the expression for $\sigma_o^{\mathrm{C}} = P_o^{\mathrm{C}}/A$ and the web is obviously not vulnerable to local buckling.

An initial run in AUTO was performed from the primary bifurcation point C, where $P = P_o^{\mathrm{C}}$ determined from the linear eigenvalue analysis, with q_s being the primary continuation parameter. Out of the many bifurcation points that were detected on the weakly stable post-buckling path, the focus was on the one with the lowest value of q_s, which is denoted as S, the so-called secondary bifurcation point. A second run was then performed from S using the branch switching function in AUTO, after which the equilibrium path exhibits the interaction between the overall and the local modes.

Figure 6 shows a plot of the normalized axial load $p = P/P_o^{\mathrm{C}}$ versus the generalized coordinates of the sway component q_s (Figure 6(a)) and the maximum out-of-plane deflection of the buckled flange plate, $w_{\max}$ (Figure 6(b)) whereas the plot in Figure 6(c) shows the relative amplitudes of the overall and the local buckling modes. Finally, the plot in Figure 6(d) shows the relationship between q_s and q_t and it can be seen that they are almost equal indicating that the shear strain is small but, importantly, not zero.

One of the most distinctive features of the equilibrium paths, Figures 6(a) and 6(b), is the sequence of snap-backs that effectively separate the equilibrium path into 11 individual parts in total as shown. The fourth, seventh and the eleventh paths are labelled as $C4$, $C7$ and $C11$ respectively in Figure 6. Each path corresponds to the formation of a new local displacement peak or trough. Figure 7 illustrates the corresponding progression of the numerical solutions for the local buckling functions w and u from path $C1$ to $C11$, where $C1$ represents the initial interactive buckling equilibrium path generated from S. It is observed that the local buckling mode is initially localized at the midspan of the column, then the buckling deformation spreads towards the supports as new peaks and troughs are formed. Figure 8 shows a selection of 3-dimensional representations of the deflected column that include the components of overall buckling (q_s and q_t) and local buckling (w and u) at a specific state on paths $C1$, $C4$, $C7$ and $C11$. As the equilibrium path develops to $C11$, the maximum out-of-plane deflection $w_{\max}$ approaches a value of 2.5 mm which is roughly twice the flange thickness and can be regarded as large in terms of geometric assumptions. The interactive buckling pattern becomes effectively periodic on path $C11$. Any further deformation along the equilibrium path would be expected to cause restabilization to the system since the boundaries would begin to confine the spread of the buckling deformation. It should be stressed of course that any plastic deformation during the loading stage would destabilize the system significantly. Figure 9 shows the direct strain, ε_z in the extreme fibre of both the vulnerable and the non-vulnerable outstands at a specific state on paths $C1$, $C4$, $C7$ and $C11$. It can be seen that the direct strain in the non-vulnerable part of the

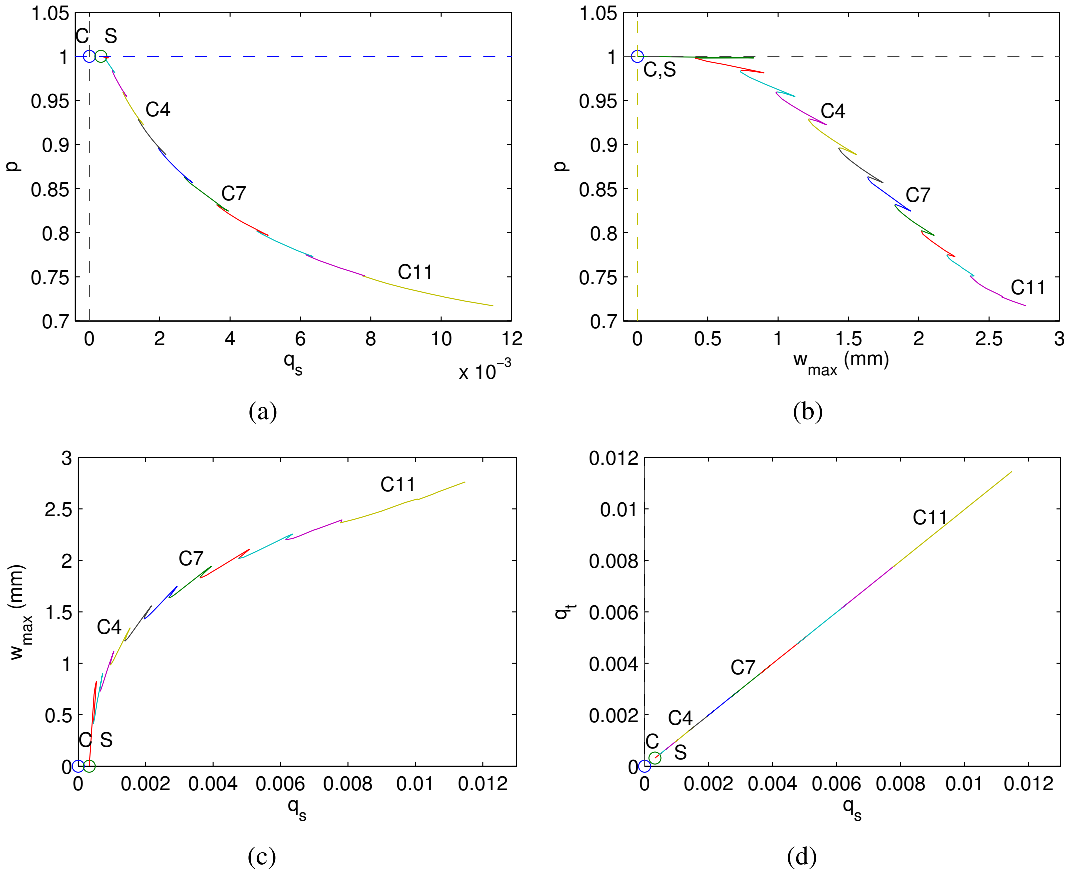

Figure 6: Numerical equilibrium paths. Graphs of the normalized force ratio p versus 6(a) the generalized coordinate q_s and 6(b) the maximum out-of-plane deflection of the buckled flange plate $w_{\max}$ are shown. The graph in 6(c) shows $w_{\max}$ versus q_s and the graph in 6(d) shows the relationship between the generalized coordinates q_t and q_s defining Euler buckling during interactive buckling.

flange has become tensile at $C11$ due to bending, whereas the maximum direct strain in the vulnerable part of the flange is approximately $1.3 \times 10^{-3} (= 0.13\%)$. This is shown to be confined to the ends of the column and is also well below the yield strain of most structural steels; even for the stainless steels given in [2], significant nonlinear softening only begins from approximately 0.1% strain.

The phenomenon described above is known in the literature as "cellular buckling" [10] or "snaking" [11]. The term "cellular buckling" was coined since it describes the way that the buckling deformation spreads in cells with progressively reduced wavelengths. The term "snaking" was coined since the equilibrium diagram exhibits progressive destabilization and restabilization, which in some other applications resembles the shape of a snake. In the current case, the destabilization is caused primarily by the interaction of the overall and local instabilities, whereas the restabilization is caused by the stretching of the buckled plates when they bend into a double curvature. As the amplitude of the overall buckling mode q_s increases, the compressive bend-

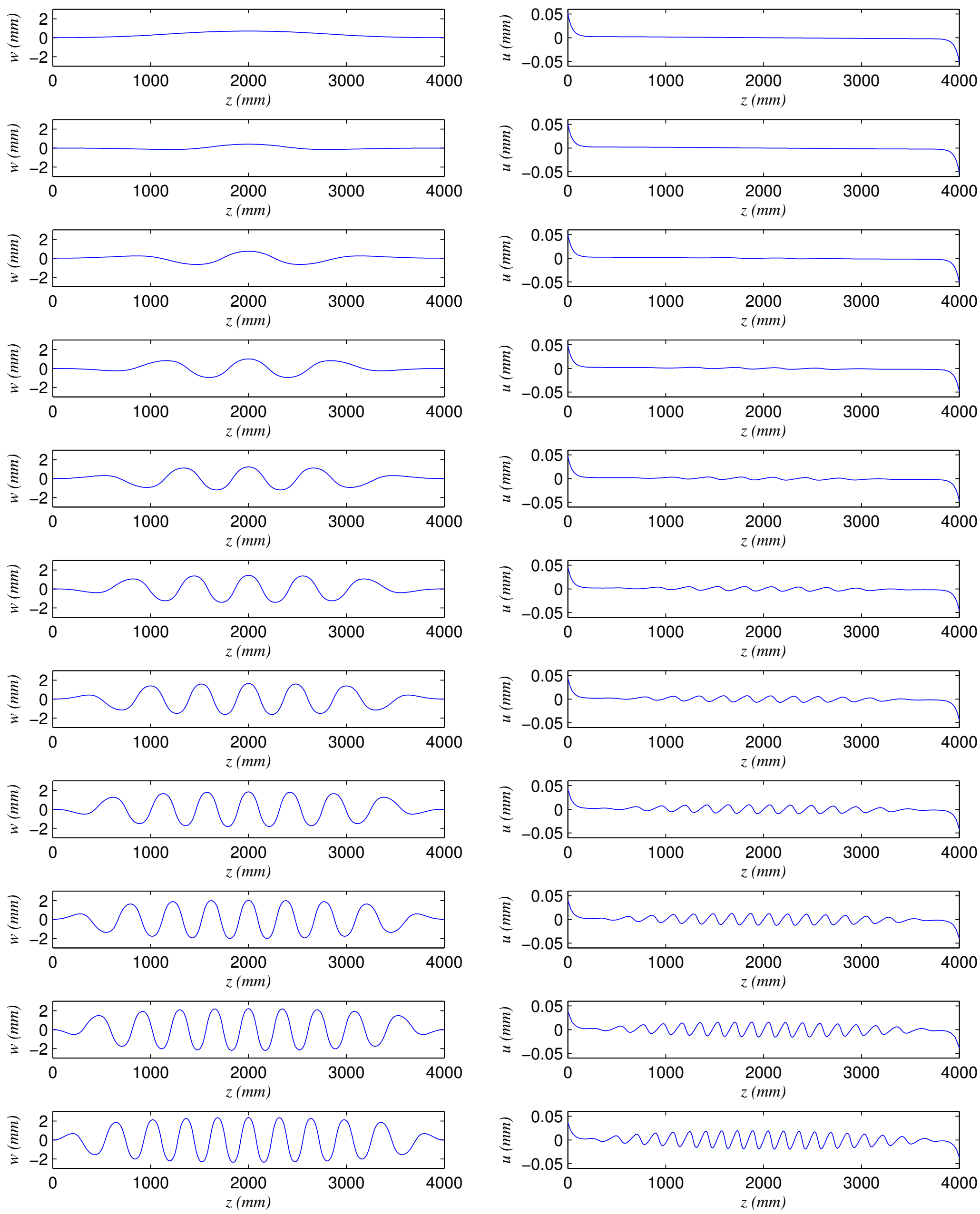

Figure 7: Numerical solutions for the local out-of-plane deflection w (left) and local in-plane deflection u (right) for the tip ($x = -b/2$) of the vulnerable flange. Individual solutions on equilibrium paths $C1$ to $C11$ are shown in sequence from top to bottom respectively.

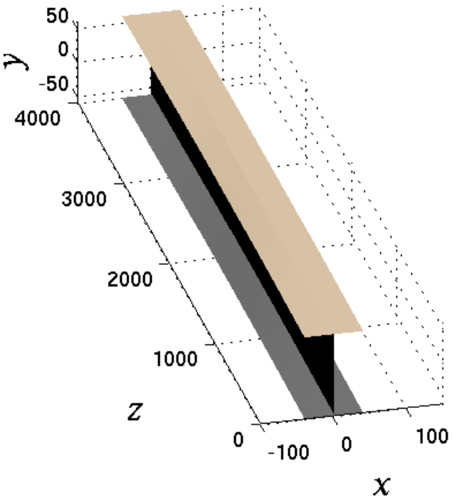

(a) $C1$: $p = 0.9988$

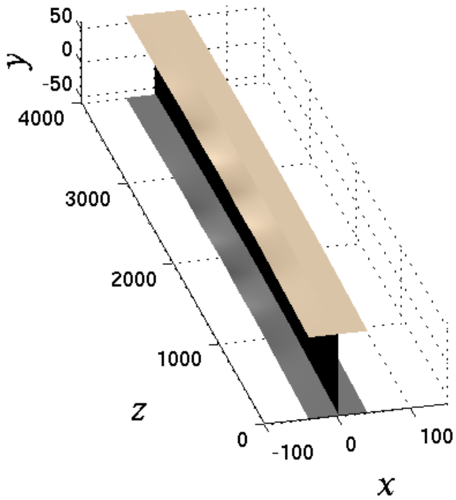

(b) $C4$: $p = 0.9597$

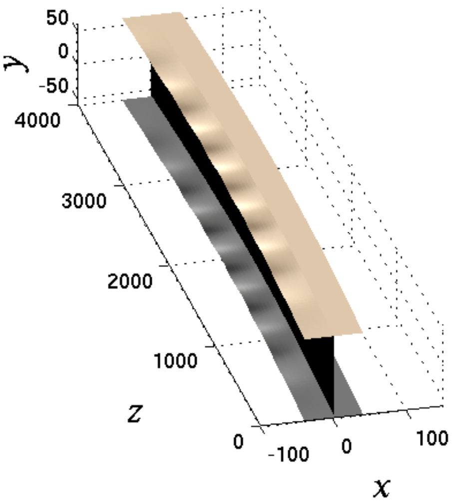

(c) $C7$: $p = 0.8635$

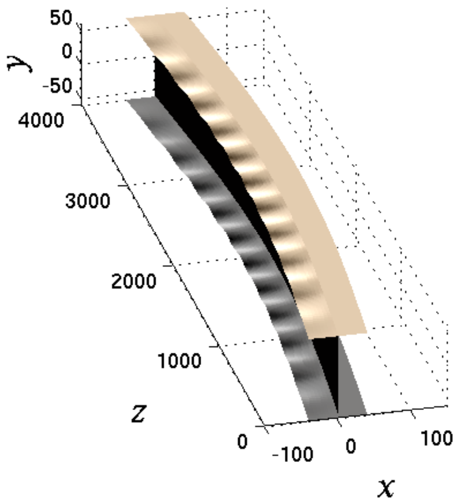

(d) $C11$: $p = 0.7511$

Figure 8: Numerical solutions of the system of equilibrium equations visualized on three dimensional representation of the column. The results are shown for individual points on paths $C1$, $C4$, $C7$ and $C11$ with the specific force ratio p given. All dimensions are in millimetres.

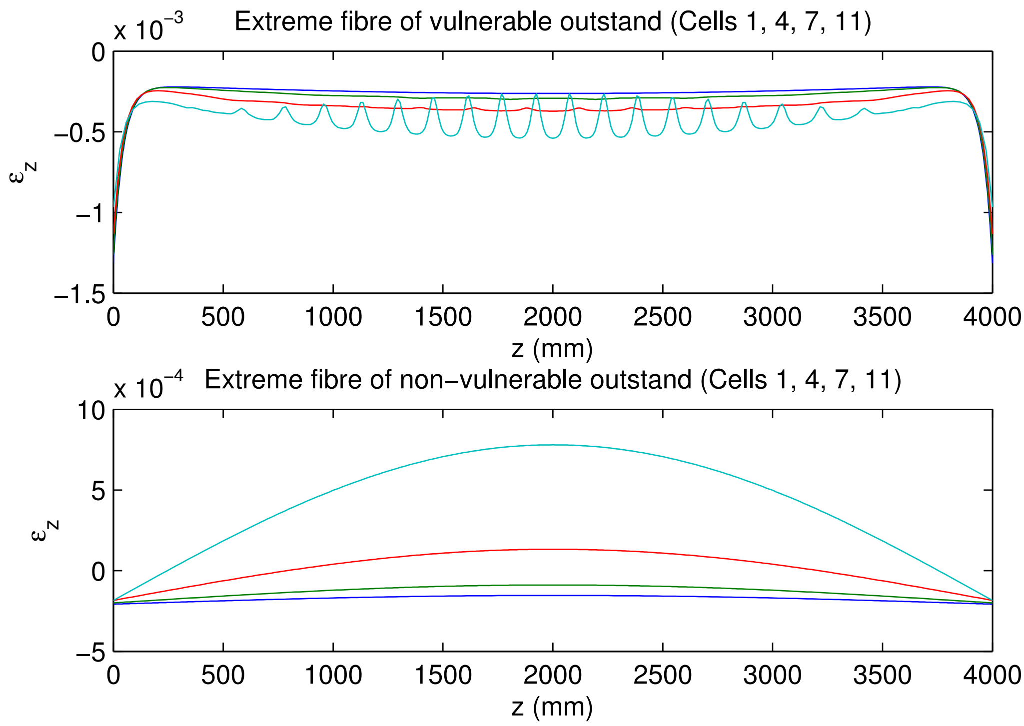

Figure 9: Direct strain ε_z in the extreme fibre of the more compressed and the less compressed outstands according to a specific point on paths $C1$ (lowest strain magnitudes), $C4$, $C7$ and $C11$ (highest strain magnitudes).

ing stress in the flange outstands increase also, which imply that progressively longer parts of the flange are susceptible to local buckling. Since local buckling is inherently stable, the drop in the load from the unstable mode interaction is limited owing to the stretching of the plate when it buckles in progressively smaller wavelengths. Therefore the cellular buckling occurs due to the effective trade-off between the unstable mode interaction and stable local buckling.

3.1 Preliminary comparison with published experiment

Figure 6 shows that the trend for both the overall lateral displacement and the local out-of-plane displacement increase as the load decreases. This indicates that the destabilization from mode interaction is stronger than the stabilizing effect of plate buckling. In terms of a preliminary comparison with an experiment, the results for the interactive buckling mode profiles in [2, 3] are compared with the specific result presented above. First of all, the interactive buckling wavelength is defined in Figure 10. The results from Figure 7 show the evolution of the interactive buckling mode. The actual experimental response, which obviously includes initial geometric imperfections, is likely to jump to the final cell relatively rapidly once the initial instability is triggered. This was shown in the experiments presented for work on the interactive

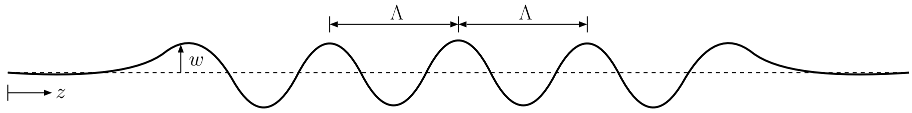

Figure 10: Definition of local buckling wavelength Λ from results for w from the variational model.

buckling of beams [4] in the cases where overall and local buckling were triggered at similar load levels. In [2] the local buckling mode has a plate buckling wavelength of 275 mm with a modulated amplitude. The numerical results in the current work show that the value of $\Lambda = 280$ mm for the interactive buckling wavelength. This close comparison offers grounds for optimism for the future developments of the current model.

3.2 Future model enhancements

Currently, the model has been developed such that the overall mode is assumed to occur before any local buckling. This is perfectly good for long columns, but for columns of intermediate to shorter lengths the possibility of local buckling occurring first would need to be accounted for. For that case, both sides of the flange outstand would be seen to buckle with q_s being initially zero. Becque and Rasmussen [2] state that their experiments show exactly this type of response for their experiments with smaller length specimens. A straightforward way of incorporating the possibility of local buckling being critical is to introduce an extra set of the local mode displacement functions. Therefore, instead of having $u(x, z)$ and $w(x, z)$ describing the local displacement of a flange outstand under more compression from flexural buckling, there would be $u_1(x, z)$ and $w_1(x, z)$ that describe that flange outstand alongside $u_2(x, z)$ and $w_2(x, z)$ that describe the flange outstand less compression from flexural buckling (see Figure 11). Moreover, the possibility of modelling the whole flange buckling locally, which would occur when local buckling is critical, would become a reality.

4 Concluding remarks

A nonlinear analytical model based on variational principles has been presented for axially-loaded thin-walled columns buckling about the weak axis. The model identifies a secondary instability which leads to highly unstable cellular buckling through a series of snap-back instabilities that result from the increasing overall buckling mode forcing the flanges to buckle locally and progressively. This process has been observed in recent experimental work and in other components that suffer from a nonlinear interaction between overall and local buckling. A preliminary comparison with a published experiment offers encouragement to pursue this analytical approach that would allow the study of the parameters that drive the behaviour.

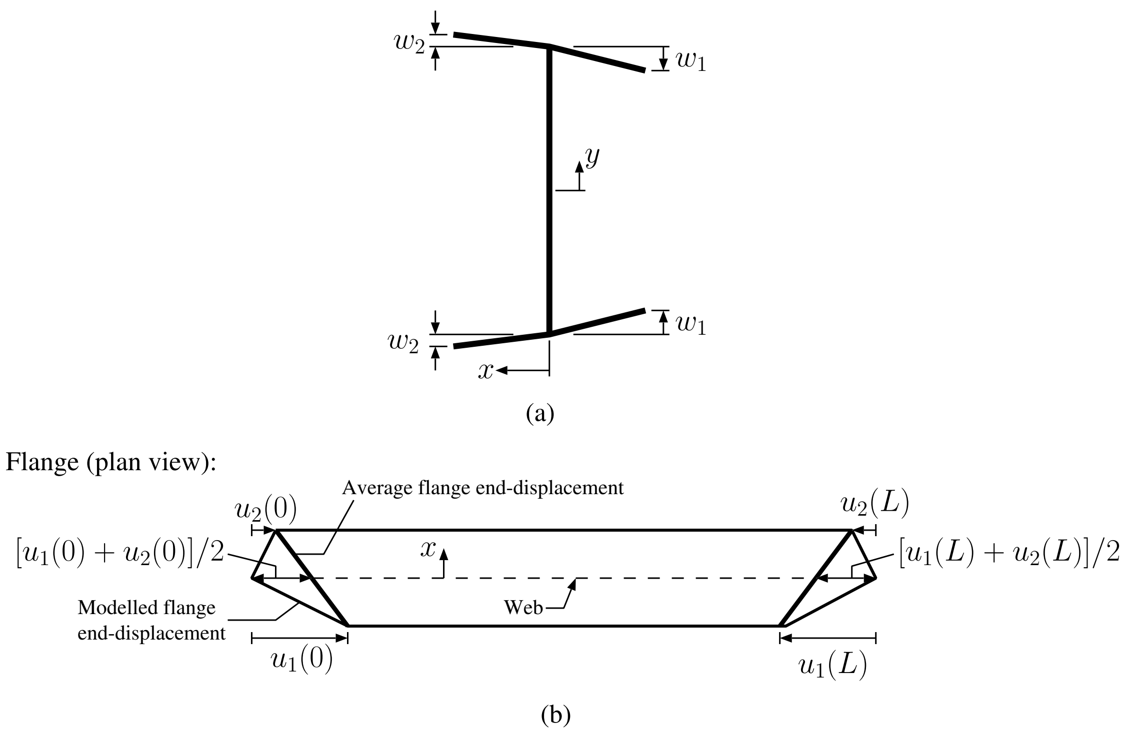

Figure 11: Model capable of accounting for local buckling being critical. (a) Out-of-plane flange outstand displacements w_1 and w_2. (b) In-plane flange outstand displacements u_1 and u_2. Similar assumptions apply as for the current model.

References

[1] S.P. Timoshenko, J.M. Gere, *Theory of elastic stability*, McGraw-Hill, New York, USA, 1961.

[2] J. Becque, K.J.R. Rasmussen, "Experimental investigation of the interaction of local and overall buckling of stainless steel I-columns", *ASCE J. Struct. Eng*, 135(11): 1340–1348, 2009.

[3] J. Becque, K.J.R. Rasmussen, "Numerical investigation of the interaction of local and overall buckling of stainless steel I-columns", *ASCE J. Struct. Eng*, 135(11): 1349–1356, 2009.

[4] M.A. Wadee, L. Gardner, "Cellular buckling from mode interaction in I-beams under uniform bending", *Proc. R. Soc. A*, 468: 245–268, 2012.

[5] G.W. Hunt, M.A. Wadee, "Localization and mode interaction in sandwich structures.", *Proc. R. Soc. A*, 454(1972): 1197–1216, 1998.

[6] W.T. Koiter, M. Pignataro, "A general theory for the interaction between local and overall buckling of stiffened panels", Tech. rept. WTHD 83, Delft University of Technology, Delft, The Netherlands, 1976.

[7] M. Pignataro, M. Pasca, P. Franchin, "Post-buckling analysis of corrugated panels in the presence of multiple interacting modes", *Thin-Walled Struct.*, 36(1): 47–66, 2000.

[8] J.M.T. Thompson, G.W. Hunt, *A general theory of elastic stability*, Wiley, London, 1973.

[9] E.J. Doedel, B.E. Oldeman, "AUTO-07P: Continuation and bifurcation software for ordinary differential equations", Technical report, Department of Computer Science, Concordia University, Montreal, Canada, 2009, Available from `http://indy.cs.concordia.ca/auto/`.

[10] G.W. Hunt, M.A. Peletier, A.R. Champneys, P.D. Woods, M.A. Wadee, C.J. Budd, G.J. Lord, "Cellular buckling in long structures", *Nonlinear Dyn*, 21(1): 3–29, 2000.

[11] J. Burke, E. Knobloch, "Homoclinic snaking: Structure and stability", *Chaos*, 17(3): 037102, 2007.

[12] G.W. Hunt, G.J. Lord, M.A. Peletier, "Cylindrical shell buckling: A characterization of localization and periodicity", *Discrete Contin. Dyn. Syst.-Ser. B*, 3(4): 505–518, 2003.

[13] M.A. Wadee, R. Edmunds, "Kink band propagation in layered structures", *J. Mech. Phys. Solids*, 53(9): 2017–2035, 2005.

[14] P.S. Bulson, *The stability of flat plates*, Chatto & Windus, London, UK, 1970.